

<https://doi.org/10.1038/s42003-024-07328-6>

# RBM4-mediated intron excision of *Hsf1* induces BDNF for cerebellar foliation

Chiu-Lun Shen<sup>1,2</sup>, Yu-Young Tsai<sup>1,4</sup>, Shen-Ju Chou<sup>3</sup>, Yao-Ming Chang<sup>1</sup> & Woan-Yuh Tarn<sup>1</sup>✉

Brain-derived neurotrophic factor (BDNF) plays important roles in brain development and neural function. Constitutive knockout of the splicing regulator RBM4 reduces BDNF expression in the developing brain and causes cerebellar hypoplasia, an autism-like feature. Here, we show that *Rbm4* knockout induced intron 6 retention of *Hsf1*, leading to downregulation of HSF1 protein and its downstream target BDNF. RBM4-mediated *Hsf1* intron excision regulated BDNF expression in cultured granule cells. Ectopic expression of HSF1 restored cerebellar foliation and motor learning of *Rbm4*-knockout mice, indicating a critical role for RBM4-HSF1-BDNF in cerebellar foliation. Moreover, N-methyl-D-aspartate receptor (NMDAR) signaling promoted the expression and nuclear translocation of RBM4, and hence increased the expression of both HSF and BDNF. A short CU-rich motif was responsible for NMDAR- and RBM4-mediated intron excision. Finally, RBM4 and polypyrimidine tract binding (PTB) proteins play antagonistic roles in intron excision, suggesting a role for splicing regulation in BDNF expression.

Alternative splicing of eukaryotic mRNA transcripts plays a critical role in diverse cellular processes, cell differentiation, and development<sup>1</sup>. Dysregulation of splicing is linked to a variety of developmental disorders and genetic or acquired diseases<sup>2</sup>. Alternative splicing occurs at high frequency in brain tissues and contributes to various steps of nervous system development, including cell-fate decisions, neuronal cell migration, and activity-regulated axon guidance and synaptogenesis<sup>3–6</sup>.

Molecular genetics and RNA sequencing have advanced our understanding of the physiological significance and disease implications of alternative splicing. Knockout of individual splicing regulators has revealed how alternative splicing events contribute to neuronal development and how impairment of splicing regulation may lead to neurodevelopmental disorders. For example, knockout of splicing regulator nSR100/SRRM4 impairs neurite outgrowth and axon guidance during nervous system development<sup>7,8</sup>. Reduction in nSR100 causes microexon skipping in a set of genes implicated in autism spectrum disorders<sup>9</sup>. Sequential expression of two polypyrimidine tract binding (PTB) protein paralogs, PTBP1 and PTBP2, in progenitor and differentiated neuronal cells is critical for brain development; they exert overlapping, but distinct functions in splicing regulation<sup>10,11</sup>. Recently, single-cell RNA-seq has revealed that splicing regulatory programs differ across neuronal types due to differential distributions of splicing regulators<sup>12</sup>. An integrative single-cell and spatial transcriptomic analysis on tumors revealed that splicing changes are associated with cancer cell differentiation and drug response<sup>13</sup>.

The RNA binding motif 4 (RBM4) protein is a ubiquitously expressed splicing regulator. RBM4 promotes neuronal differentiation via regulating splice isoform expression of the Notch signaling inhibitor Numb and metabolic enzyme pyruvate kinase M in cultured neural progenitor cells and mesenchymal stem cells<sup>14,15</sup>. An *in utero* study shows that RBM4 contributes to the expression of full-length Dab, which is critical for the radial migration of newborn neurons<sup>16</sup>. Notably, RBM4 regulates the expression of PTBP1/PTBP2 proteins via splicing control and antagonizes their activity in splicing regulation<sup>4,17</sup>. Together, these studies indicate that RBM4 plays a significant role in the development of the nervous system.

RBM4 is encoded by two copies of *Rbm4* genes (a and b) that are located adjacently on the same chromosome. Constitutive *Rbm4a/Rbm4b* double gene-knockout (*Rbm4dKO*) mice exhibit cerebellar foliation defects, particularly in vermal lobules VI and VII<sup>18</sup>. The absence of the intercrural fissure (icf) between these two lobules is a feature of autistic individuals<sup>19</sup>. *Rbm4* knockout reduces the expression of brain-derived neurotrophic factor (BDNF) in the developing brain<sup>18</sup>. BDNF reduction compromises tropomyosin-related kinase receptor type B (TrkB) signaling. TrkB agonist 7,8-dihydroxyflavone can stimulate BDNF expression and restore icf formation, indicating the critical role of BDNF in cerebellar foliation.

To explore how RBM4 regulates BDNF expression during brain development, we have performed RNA-seq in *Rbm4dKO* embryonic brains<sup>18</sup>. In this study, we found that RBM4 promoted HSF1 expression by removing its retained intron from the transcript and that its splicing activity

<sup>1</sup>Institute of Biomedical Sciences, Academia Sinica, Taipei, Taiwan. <sup>2</sup>Institute of Molecular Medicine, College of Medicine, National Taiwan University, Taipei, Taiwan. <sup>3</sup>Institute of Cellular and Organismic Biology, Academia Sinica, Taipei, Taiwan. <sup>4</sup>Present address: Columbia University in the City of New York, New York, USA. ✉e-mail: [wtarn@ibms.sinica.edu.tw](mailto:wtarn@ibms.sinica.edu.tw)

was regulated by neuronal signaling. Importantly, HSF1 upregulated BDNF expression and rescued cerebellar foliation and motor learning of *Rbm4* knockout. This study provides mechanistic insights into how RBM4 exerts splicing control to ensure proper cerebellar development and behaviors.

## Results

### *Rbm4* knockout affects alternative splicing in the embryonic brain

RNA-seq analysis of wild-type and *Rbm4*dKO brains at embryonic day 13.5 (E13.5) was previously performed<sup>19</sup>, revealing ~1100 alternative splicing events (false discovery rate <0.005 from replicate Multivariate Analysis of Transcript Splicing) in ~900 genes (Supplementary Data 1 for rMATS of RNA-seq data). Among them, ~45% of the events ( $n = 498$ ) were cassette exon selection (CES) and, surprisingly, ~42% ( $n = 464$ ) were differential intron retention (IR) (Fig. 1A). In the CES category, *Rbm4* knockout resulted in 56% ( $n = 278$ ) exon inclusion and 44% ( $n = 220$ ) exon exclusion (Fig. 1B). Gene Ontology (GO) enrichment analysis was performed using Database for Annotation, Visualization and Integrated Discovery

(DAVID), showing that top enriched biological processes of RBM4-regulated genes in the CES category included RNA processing, muscle contraction and calcium transport (Fig. 1C). Calcium transport was notable because it is critical for the neuronal development and activity<sup>20</sup>. Unexpectedly, *Rbm4* knockout caused differential IR (97.2% upregulated and 2.8% downregulated) in a substantial portion of target transcripts (Fig. 1D). The most affected transcripts encoded factors involved in RNA processing/splicing and ribosome biogenesis (Fig. 1E). Retained introns in *Rbm4*dKO brain are shorter and have a slightly higher GC content than average (Fig. 1F, G), consistent with a report that short and GC-rich introns retain introns more frequently<sup>21</sup>.

### RBM4 modulates target protein expression via regulated intron excision

Next, we selected several target transcripts relevant to neuronal functions in the CES category for verification, including calcium transport and signaling factors (*Cacna1d*, *Camk2b*, *Camk2g*, and *Ryr2*) and factors controlling synaptic activity and synaptogenesis (*Nav2* and *Nrxn2*). *Rbm4* knockout

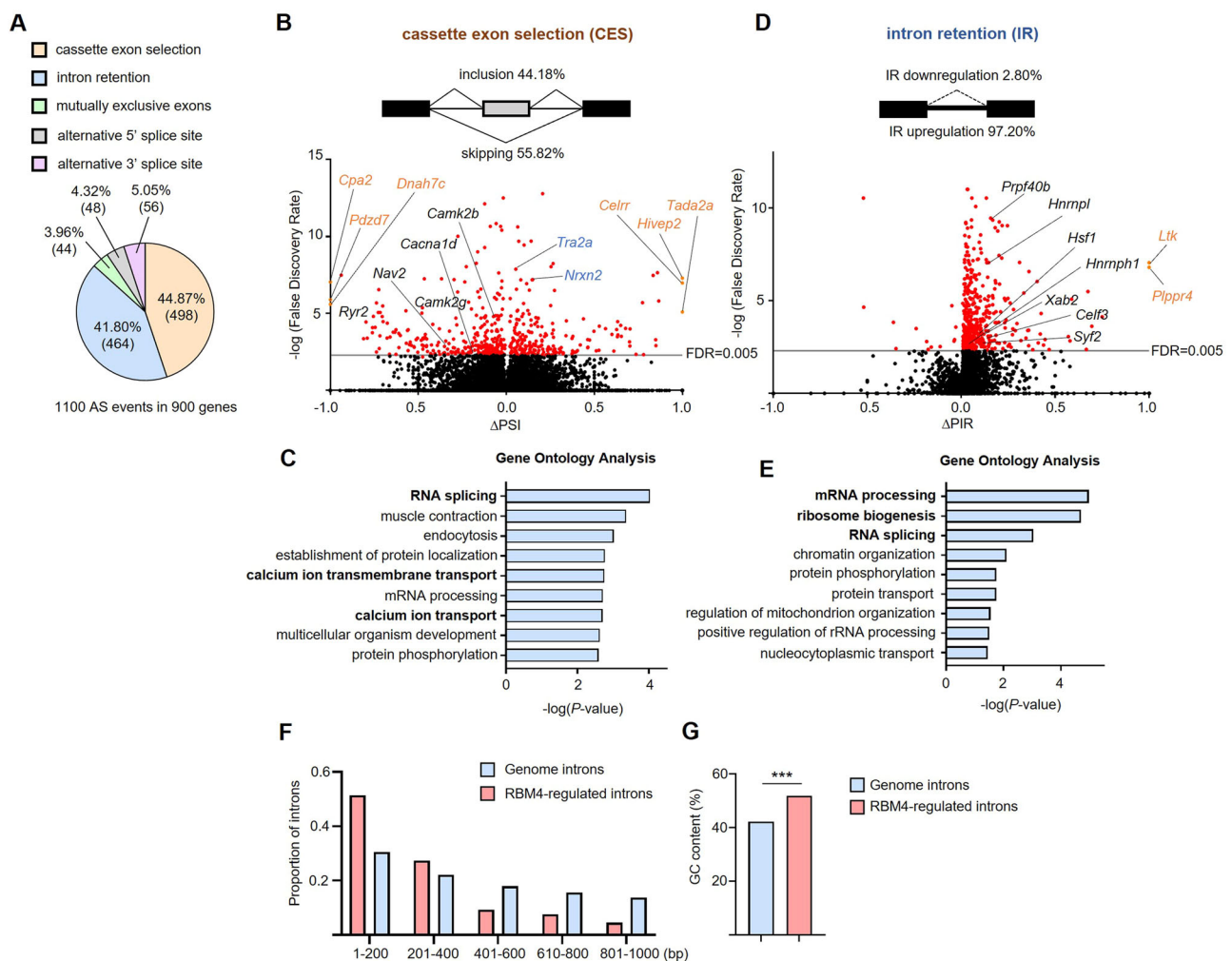


**Fig. 1 | RNA-seq analysis of *Rbm4*dKO embryonic brain.** **A** Pie chart shows alternative splicing events identified in the E13.5 *Rbm4*dKO brain. The percentage and event number of each category are indicated. **B** Schematic depicts cassette exon selection (CES). Volcano plot of CES: the x-axis represents the difference of percent spliced in ( $\Delta$ PSI:  $\text{PSI}^{\text{Rbm4dKO}} - \text{PSI}^{\text{WT}}$ ); the y-axis indicates the negative log<sub>10</sub> transformation of false discovery rate (FDR). Red dots represent differentially expressed CES events with statistical significance (FDR < 0.005). Transcripts indicated were subjected to RT-PCR analysis (see Fig. 2) (black, exon skipping; blue, exon inclusion). Orange indicates the transcripts with a  $\Delta$ PSI value of 1.0 or -1.0. **C** Gene Ontology analysis of the CES category. The x-axis represents the negative log<sub>10</sub>

transformation of the  $P$ -value; the y-axis indicates the top-ranked terms in the CES category. **D** Schematic depicts intron retention (IR). Volcano plot of the IR category: the x-axis indicates the difference in percent intron retention ( $\Delta$ PIR:  $\text{PIR}^{\text{Rbm4dKO}} - \text{PIR}^{\text{WT}}$ ); the y-axis is the same as in (B). Red dots represent differentially expressed IR events with FDR < 0.005. Orange indicates the transcripts with a  $\Delta$ PIR value of 1.0. **E** Gene Ontology analysis of the IR category; the x-axis is the same as in (C); the y-axis indicates the top-ranked terms in the IR category. **F** Intron length distribution comparison between genome introns ( $n = 490290$ ) and RBM4-regulated introns ( $n = 399$ ). **G** The GC content of genome introns and RBM4-regulated introns. Bars represent average  $\pm$  SEM (\*\* $P < 0.001$ ).

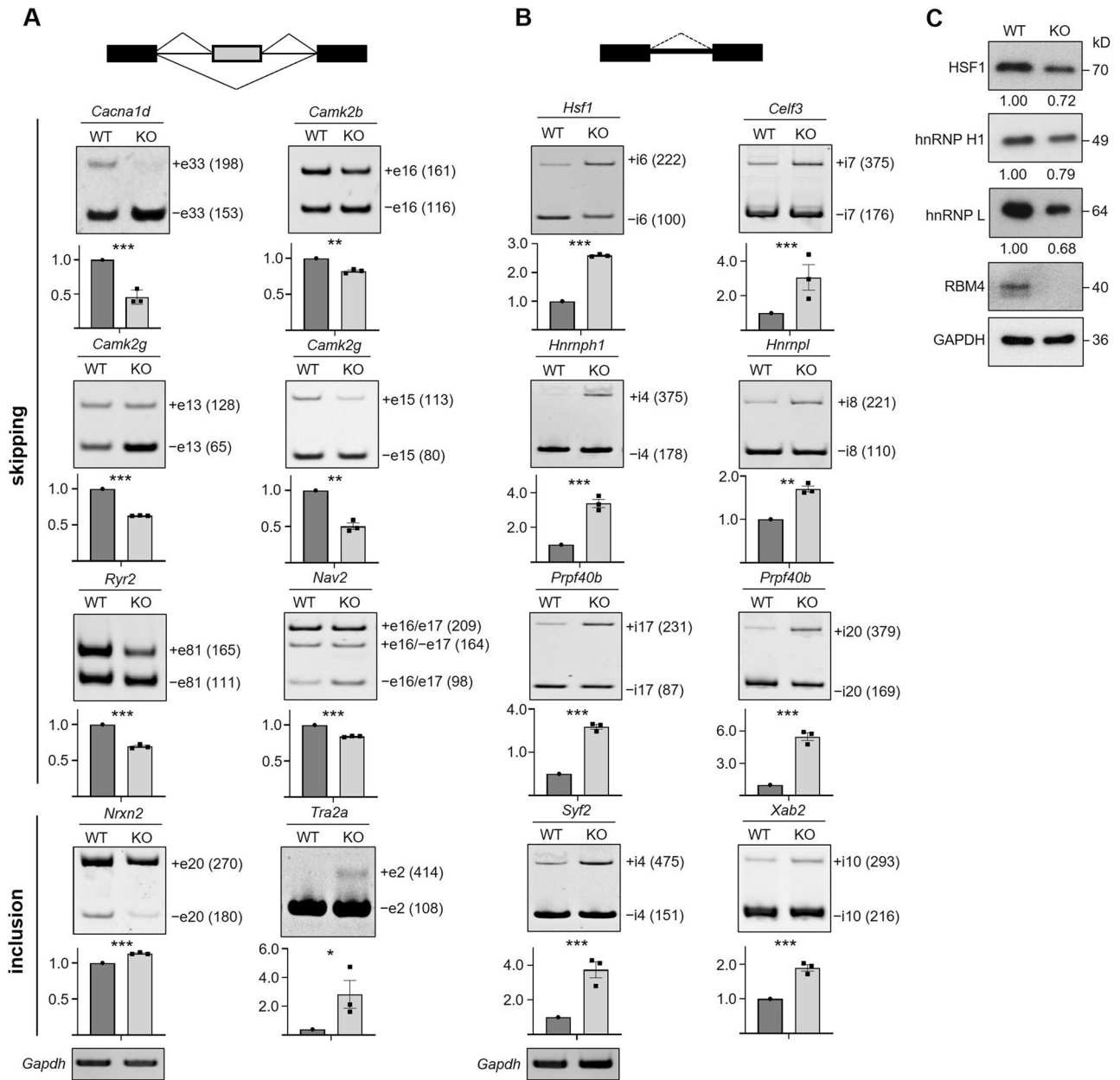


**Fig. 2 | *Rbm4* knockout affects cassette exon selection and causes intron retention.** **A** RT-PCR of selected RBM4 targets in the CES category from E13.5 wild-type (WT) and *Rbm4* knockout (KO) brains. Bar graphs show relative PSI (+e/total); WT was set to 1 ( $n = 3$ ). GAPDH was used as a loading control. **B** RT-PCR of selected RBM4 targets in the IR category from E13.5 brains. Bar graphs show relative PIR (+i/total); WT was set to 1 ( $n = 3$ ). *P*-values were determined using the Student's *t*-test.

$*P < 0.05$ ,  $**P < 0.01$ ,  $***P < 0.001$ . The number in parentheses represents basepair (bp). **C** Immunoblotting shows three selected proteins (HSF1, hnRNP H1, hnRNP L) in E13.5 WT and KO brain lysates. The level of examined proteins was normalized to GAPDH. Numbers below the blots indicate relative protein level (WT was set to 1;  $n = 3$ ). *P*-values are listed in Supplementary Data 2.

resulted in alternative exon inclusion in *Nrxn2* and skipping in all other transcripts tested (Fig. 2A, and Supplementary Fig. 1A for the sashimi plots), consistent with RNA-seq data (Fig. 1B). Alternative splicing segment-4 (ASS4) of neurexins determines their binding preference to postsynaptic partners<sup>22</sup>. Depolarization-dependent CES of neurexins has been detected in cerebellar neurons<sup>23</sup>. *Rbm4* knockout induced ASS4 (exon 20) inclusion of *Nrxn2*, suggesting a role for RBM4 in modulating synaptic activity. Notably, RNA metabolism, particularly splicing regulation, was overrepresented in both CES and IR categories. For example, *Rbm4* knockout induced the inclusion of poison exon 2 in *Tra2a*, which triggers nonsense-mediated mRNA decay (NMD)<sup>24</sup>. More strikingly, *Rbm4* knockout caused IR of a large set of transcripts encoding RNA binding proteins (Fig. 2B and

Supplementary Fig. 1B, *Celf3*, *Hnrnp1*, *Hnrnp1*, *Prpf40b*, *Syf2*, and *Xab2*), as reported in erythrocytic and B-lymphoblastic cells<sup>25,26</sup>. The expression level of the above genes except for *Hnrnp1* and *Tra2a* was not significantly changed (Supplementary Fig. 1C).

The heat-shock factor HSF1 is a transcriptional activator for heat-shock protein genes and has been implicated in *Bdnf* expression<sup>27</sup>. *Rbm4* knockout also increased IR of *Hsf1* (Fig. 2B and Supplementary Fig. 1B, *Hsf1*), suggesting that RBM4 regulates BDNF expression probably via HSF1. IR has been considered a mechanism for post-transcriptionally down-regulating gene expression via NMD<sup>28,29</sup>. Therefore, we examined the level of HSF1 (the focus of this study, see below) and two hnRNP proteins (H1 and L), whose intron-containing transcripts have been detected in

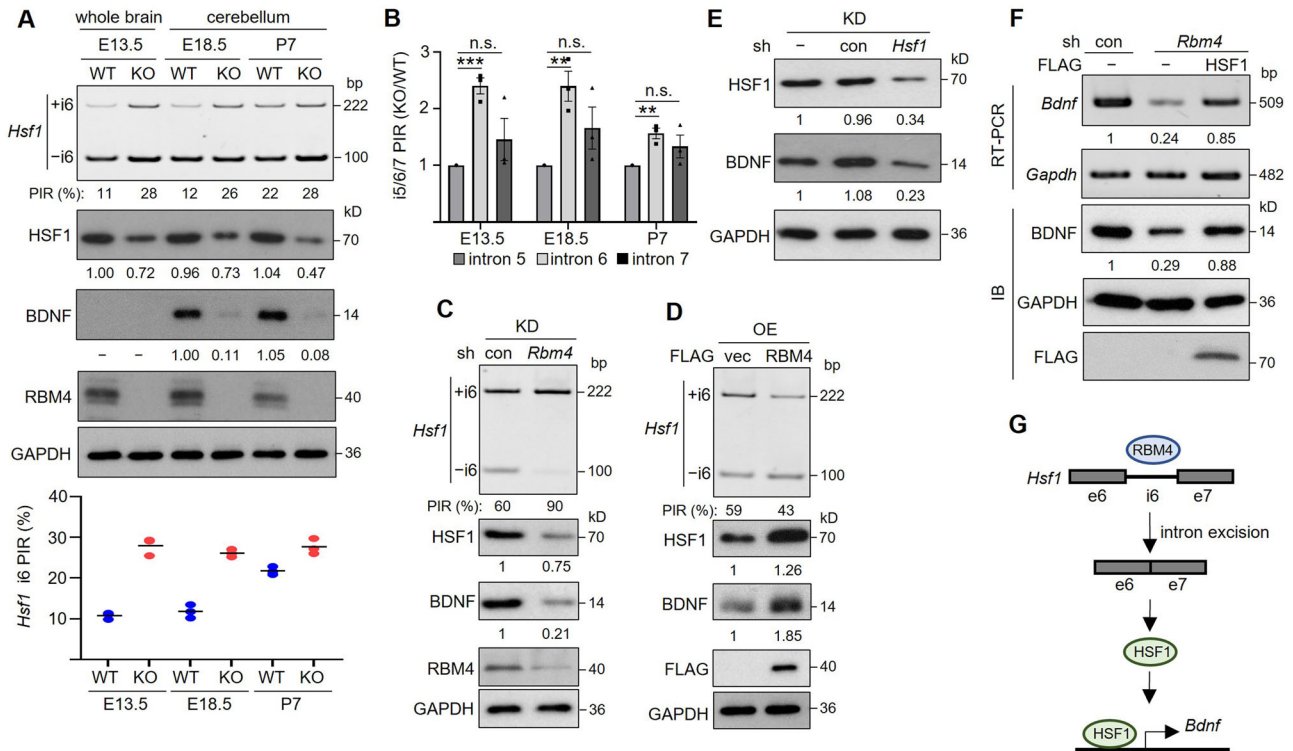


**Fig. 3 | RBM4 promoted intron 6 excision of *Hsf1* leads to *Bdnf* transactivation.** **A** RT-PCR of *Hsf1* and immunoblotting of indicated proteins in WT and KO whole brain or cerebellar lysates at different developmental stages. For splicing, PIR (%) was indicated below the gel (average from three experiments) and in the dot graph (data of three experiments). For immunoblotting, the level of each protein was normalized to GAPDH. Numbers below the blots show relative protein levels. For HSF1, E13.5 WT brain was set to 1. For BDNF, E18.5 WT cerebellum was set to 1. **B** Bar graph shows relative KO/WT PIR of *Hsf1* introns 5/6/7 at indicated time points. **C** RT-PCR of *Hsf1* and immunoblotting of indicated proteins were performed in control (con) or *Rbm4*-targeting shRNA-transfected GCs. PIR (%) and

relative protein level were as in (A). KD: knockdown. **D** RT-PCR and immunoblotting of mock (vec) or FLAG-RBM4-overexpressed GCs were performed as in (C). OE: overexpression. **E** Immunoblotting of indicated proteins was performed in control (con) or *Hsf1* shRNA-transfected GCs. Relative protein level was shown below the blots. **F** Mock (lane 1) or RBM4 knockdown GCs (lanes 2 and 3) were transfected with the empty (-) or FLAG-HSF1 expression vector. RT-PCR and immunoblotting were performed and relative RNA/protein expression levels were indicated. Lane 1 was set to 1. **G** Schematic shows that RBM4 promotes BDNF expression via removing retained intron 6 from *Hsf1*.

erythroblasts<sup>25</sup>. Immunoblotting showed that the level of all three proteins was reduced by 30–50% in the E13.5 *Rbm4*KO brain (Fig. 2C), indicating that *Rbm4* deficiency was downregulated due to IR upregulation.

Together, *Rbm4* knockout affected CES and IR to a similar extent. RBM4 may modulate neuronal activity via CES, whereas it affected the expression of RNA processing factors through both CES and IR.

**Intron excision of *Hsf1* by RBM4 enhances *Bdnf* transactivation**

We focused on *Hsf1* because it has been implicated in *Bdnf* transactivation<sup>27</sup>. First, we evaluated *Hsf1* splicing at different developmental time points. In wild-type brains, intron 6 retention was minimally detected during early developmental stages (E13.5 whole brain and P0 cerebellum) and increased in the P7 cerebellum (Fig. 3A, RT-PCR, and dot graph for WT). *Rbm4* knockout enhanced intron 6 retention and reduced HSF1 protein levels at all stages examined (Fig. 3A, KO). No significant change was detected in introns 5 and 7 in both wild-type and *Rbm4*KO brains (Fig. 3B, Supplementary Fig. 2A), suggesting that intron 6 serves as a regulatory intron for gene expression control. Immunoprecipitation-RT-PCR analysis revealed RBM4 binding to *Hsf1* transcripts in E13.5 brain lysates, suggesting that *Hsf1* is a direct target of RBM4 (Supplementary Fig. 2B). To further confirm the role of RBM4 in *Hsf1* intron 6 regulation, we knocked down RBM4 using shRNA in cultured P7 GCs. Depletion of RBM4 increased intron 6 retention of *Hsf1*, resulting in downregulation of HSF1 and BDNF proteins (Fig. 3C). In contrast, overexpression of RBM4 in GCs induced intron 6 excision, and hence increased the levels of both HSF1 and BDNF (Fig. 3D). Next, we evaluated whether HSF1 is responsible for BDNF expression. As a result of HSF1 reduction by >60%, BDNF protein levels decreased by nearly 80%

(Fig. 3E). Overexpression of FLAG-tagged HSF1 in RBM4-depleted GCs restored BDNF expression (Fig. 3F). Our results revealed that *Rbm4* deficiency caused intron retention of *Hsf1*, leading to downregulation of HSF1 and its downstream BDNF. RBM4 promoted the expression of HSF1 via splicing control, which subsequently transactivated *Bdnf* (Fig. 3G).

**HSF1 rescues the foliation defects of *Rbm4* knockout cerebellum**

Cerebellar icf formation of *Rbm4*KO mice was impaired due to BDNF deficiency and reformed by reactivation of TrkB (T1). The above results indicated that BDNF deficiency resulted from downregulation of HSF1. Therefore, it was important to evaluate whether HSF1 contributes to cerebellar foliation during brain development. We generated and injected an expression vector for DsRed (control; dKO<sup>con</sup>) or HSF1-DsRed (dKO<sup>HSF1</sup>) into the lateral ventricle of E15.5 *Rbm4*KO followed by electroporation (Fig. 4A, the detailed procedure is described in the “Methods” section). We observed DsRed expression in the external granule layer of the cerebellum, primarily overlapping with GCs, in the injected *Rbm4*KO newborns (Supplementary Fig. 3A and 3B for magnified images). Immunoblotting confirmed that HSF1-DsRed was expressed in the P0 *Rbm4*KO<sup>HSF1</sup> cerebellum at a level comparable to endogenous HSF1 in the wild-type. Importantly, BDNF mRNA and protein, as well as calbindin, were fully recovered at P0 (Fig. 4B). Moreover, HSF1 was sufficient to restore cerebellar foliation as early as P0 and icf formation at P30 (Fig. 4C, D). Similar results were observed with the injection in the fourth ventricle, where cerebellar precursor cells are more abundant (Supplementary Fig. 3C, D). Finally, we evaluated the motor learning of *Rbm4*KO<sup>HSF1</sup> mice using rotarod analysis. During pretraining at a constant low speed, the

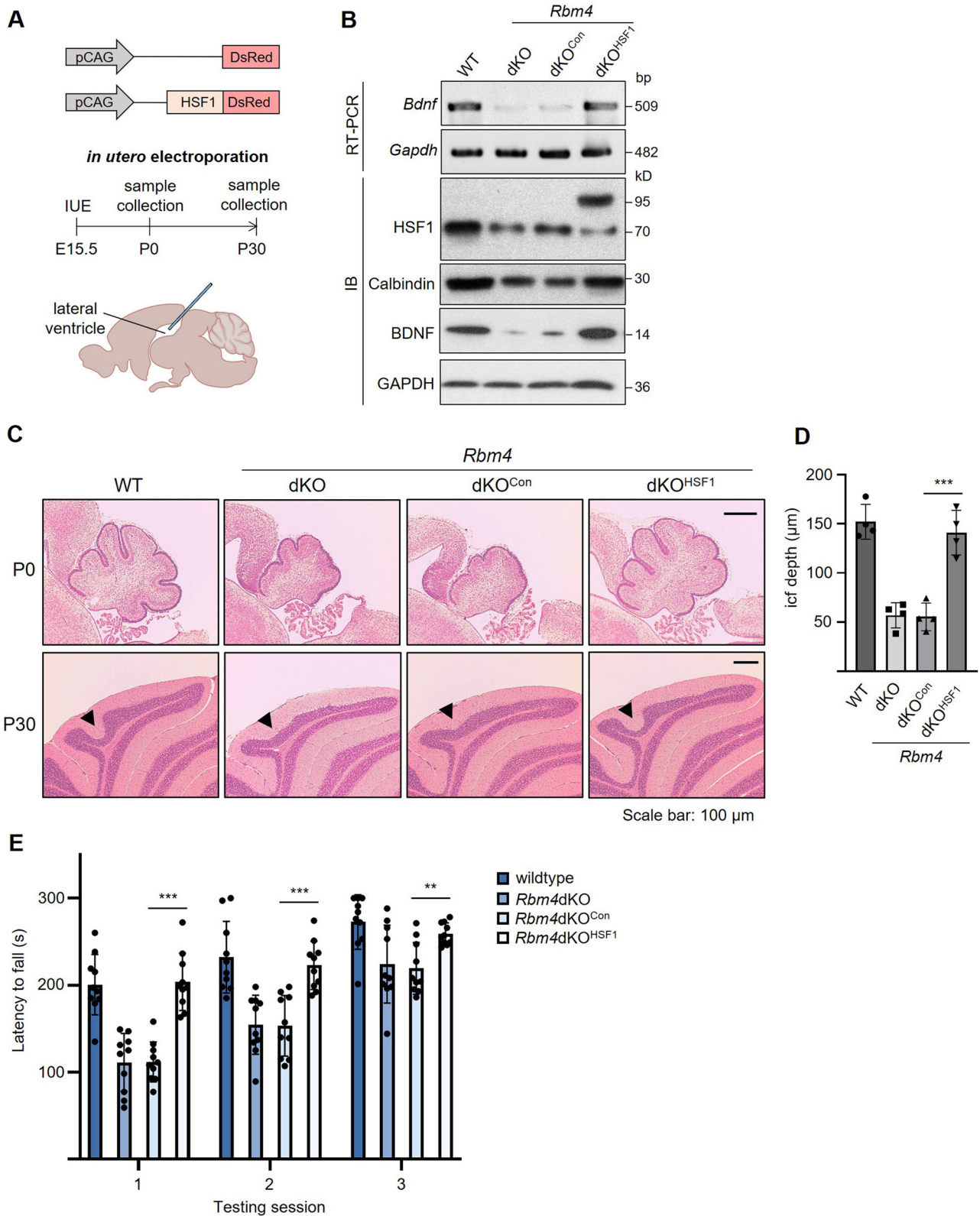


**Fig. 4 | HSF1 rescues the foliation defects of the *Rbm4* knockout cerebellum.**

**A** Schematic diagram shows the construct of the DsRed (Con) and HSF1-DsRed fusion, and the procedure of *in utero* electroporation (IUE). The empty or HSF1-DsRed plasmid was electroporated into the lateral ventricle of the E15.5 *Rbm4*dKO brain. Newborn pups (*Rbm4*dKO<sup>Con</sup> and *Rbm4*dKO<sup>HSF1</sup>) were sacrificed at P0 or P30. **B** The expression levels of BDNF mRNA and indicated protein were evaluated in the P0 cerebellum of wild-type (WT), *Rbm4*dKO, *Rbm4*dKO<sup>Con</sup>, and *Rbm4*dKO<sup>HSF1</sup>.

**C** Hematoxylin and eosin staining were performed in P0 and P30 cerebellums of mice as indicated. Arrowhead indicates icf. **D** The icf depth was measured in the P30 cerebellum. Bars represent average  $\pm$  SEM ( $n = 3$ , \*\*\* $P < 0.001$ ). **E** For rotarod analysis, each mouse (6-week-old) was trained on the rod for 60 s at low constant speed (Supplementary Fig. 3C) before proceeding to the tests with an accelerating rotational speed from 4 to 40 rpm over a period of 300 s. Bar graph shows the average latency to fall (s) (10 mice for each group); \*\*\* $P < 0.001$ ; \*\* $P < 0.01$ .

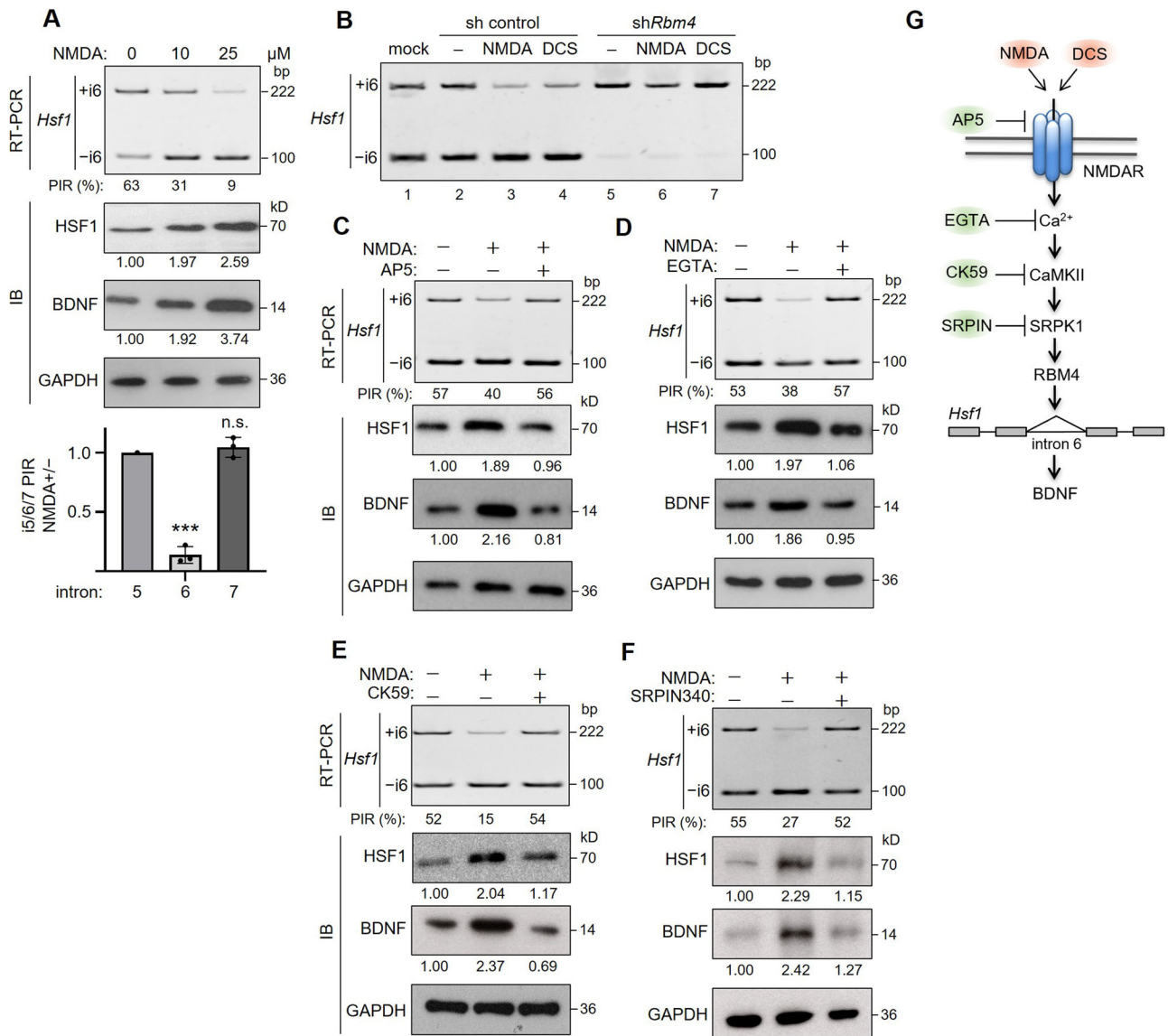


**Fig. 5 | NMDA receptor signaling regulates RBM4-mediated intron excision of *Hsf1*.** **A** GCs were treated with different concentrations of NMDA for one hour. RT-PCR of *Hsf1* and immunoblotting of HSF1, BDNF, and GAPDH were performed. PIR (%) and relative protein level were measured as in Fig. 3A. Bar graph shows *Hsf1* introns 5/6/7 PIR of 25 μM NMDA-treated (+) relative to mock-treated (-) cells (\*\**P* < 0.001; n.s. no significance). **B** GCs were transfected with the control or *Rbm4* shRNA followed by NMDA (25 μM) or DCS (50 μM) treatment. RT-PCR of *Hsf1*

was performed. Lane number is indicated below the gel. **C–F** GCs were mock-treated (-) or pre-treated with AP5 (25 μM), EGTA (2 mM), CK59 (500 nM) or SRPIN340 (30 μM) followed by NMDA treatment. RT-PCR, immunoblotting, and measurement of PIR (%) and relative protein levels were performed as in (A). **G** Schematic diagram shows that NMDAR signaling modulates RBM4-mediated *Hsf1* intron 6 splicing. Activators and inhibitors of NMDAR signaling pathways are indicated in red and green ovals, respectively.

performance of *Rbm4*dKO<sup>HSF1</sup> and wild-type mice was almost indistinguishable (Supplementary Fig. 3E). As the rotational speed accelerated, *Rbm4*dKO<sup>HSF1</sup> mice still performed significantly better than untreated *Rbm4*dKO or *Rbm4*dKO<sup>Con</sup> mice (Fig. 4E). Together, our result indicated that the RBM4-HSF1-BDNF pathway contributes to cerebellar icf formation and motor learning, although we cannot completely exclude the possibility that HSF1 also induced BDNF in other brain areas, such as the cerebral cortex and hippocampus, thereby affecting behaviors.

### NMDA receptor signaling regulates RBM4-mediated intron excision of *Hsf1*

The finding of RBM4-regulated HSF1 expression via regulated intron removal prompted us to explore how neuronal activity may influence RBM4-mediated splicing control. N-methyl-D-aspartate (NMDA) signaling plays an important role in brain development and plasticity<sup>30,31</sup>. Notably, NMDA may protect GCs against apoptosis by inducing BDNF

in the cerebellum<sup>32</sup>. *Rbm4* knockout increased caspase 3 cleavage and reduced AKT and ERK1/2 phosphorylation, indicating a pro-apoptotic status (Supplementary Fig. 4A). Treatment of GCs with lower doses of NMDA (up to 25 μM) suppressed apoptosis, whereas higher doses (50 μM) reversed it (Supplementary Fig. 4B). Within an optimal range, NMDA increased BDNF expression in a concentration-dependent manner, coinciding with the excision of intron 6—but not intron 5 or 7—of *Hsf1* and increased HSF1 protein levels (Fig. 5A, Supplementary Fig. 4C). D-cycloserine (DCS), a partial agonist of NMDA receptor (NMDAR), also induced intron 6 excision (Fig. 5B, lane 4). Importantly, the knockdown of RBM4 abolished NMDA or DCS-induced intron 6 excision (Fig. 5B, lanes 6, 7), suggesting that RBM4 is responsible for signaling-induced splicing. To confirm the role of NMDAR in *Hsf1* splicing, we treated GCs with its antagonist D-2-amino-5-phosphonopentanoate (AP5) prior to NMDA treatment. The result showed that AP5 abolished NMDA-induced intron 6 excision of *Hsf1* and increased HSF1

and BDNF proteins (Fig. 5C). Moreover, we examined the components of NMDAR signaling pathways including  $\text{Ca}^{2+}$  influx and  $\text{Ca}^{2+}$ /calmodulin-dependent protein kinases (CaMKs). Prior to NMDA treatment, GCs were treated with the metal-ion chelator EGTA or CaMKII antagonist CK59. As observed with AP5, EGTA, and CK59 also abolished the effects of NMDA on *Hsf1* splicing and HSF1 and BDNF protein expression (Fig. 5D, E). Notably, the SR protein kinase SRPK1 can act downstream of NMDAR to regulate intron excision<sup>33</sup>. Since SRPK1 can phosphorylate RBM4 *in vitro*<sup>34</sup>, we tested the effect of SRPK1 inhibition on *Hsf1* splicing. Figure 5F shows that the SRPK1 inhibitor SRPIN340 had similar effects as the above inhibitors (Fig. 5C–E). In addition, we assessed the effect of NMDAR signaling on other RBM4 targets. Supplementary Fig. 4D shows that NMDA also promoted exon inclusion of *Ryr2* and *Camk2g* and intron excision of *Celf3* and *Xab2*, contrary to that observed with *Rbm4* knockout (Fig. 2), underscoring the role of NMDAR signaling in RBM4-mediated splicing. Together, this study revealed a regulatory axis, NMDAR–CaMKII–SRPK1–RBM4, for neuronal cue-mediated splicing regulation (Fig. 5G).

### NMDAR signaling regulates the nuclear abundance of RBM4

Since NMDAR signaling had a significant impact on RBM4-mediated splicing regulation (Fig. 5), we next asked whether NMDA directly regulates the activity of RBM4. Surprisingly, NMDA treatment significantly increased the level of RBM4 protein, but not its mRNA (Fig. 6A). This effect of NMDA treatment was counteracted by AP5 or CK59, suggesting that RBM4 protein may be stabilized by the NMDAR–CaMKII pathway (Fig. 6B). RBM4 has a phosphorylation site at serine 309 (Fig. 6C)<sup>34</sup>. Substitution of this serine residue by alanine (i.e., SA mutation) abolished NMDA-induced RBM4 increase (Fig. 6C), suggesting that RBM4 was stabilized by CaMKII-induced phosphorylation. Moreover, immunofluorescence showed that NMDA treatment increased RBM4 signals in the nucleus (Fig. 6D, mock vs. NMDA/-). Subcellular fractionation confirmed that NMDA increased the level of RBM4, particularly in the nucleus, with concomitant reduction of its cytoplasmic level (Fig. 6E). Blocking NMDAR–CaMKII pathway with AP5 or CK59 reversed nuclear translocation of RBM4 (Fig. 6D). Moreover, we evaluated subcellular localization of the SA mutant of RBM4. FLAG-tagged wild-type RBM4 behaved the same as the endogenous in response to NMDA (Fig. 6F, RBM4<sup>WT</sup>). However, the SA mutant still remained in the cytoplasm after NMDA treatment (Fig. 6F, RBM4<sup>SA</sup>), indicating that NMDA-induced S309 phosphorylation not only stabilizes RBM4 but also promotes its translocation to the nucleus. Finally, we tested the functional effect of the SA mutation. Overexpression of RBM4<sup>WT</sup> in *Rbm4*ΔKO GCs restored BDNF expression, whereas RBM4<sup>SA</sup> failed to achieve (Fig. 6G). Together, our results revealed that NMDAR signaling-induced HSF1 and subsequent BDNF expression by increasing the nuclear abundance of RBM4 through phosphorylation.

### NMDAR signaling regulates RBM4-mediated *Hsf1* splicing via a CU-rich motif

Finally, we focused on the *cis*-elements responsible for RBM4-mediated IR regulation. We generated a minigene encompassing the genomic region from exon 6 to exon 8 of mouse *Hsf1* (Fig. 7A). Knockdown and overexpression of RBM4 respectively increased and reduced intron 6 retention but had no significant effect on intron 7 (Fig. 7B, Supplementary Fig. 5A). NMDA or DCS also specifically promoted the excision of intron 6, but not intron 7, of the *Hsf1* minigene (Fig. 7C, Supplementary Fig. 5B), indicating that this minigene behaved similarly as endogenous *Hsf1* (Fig. 5). RBM4 regulates alternative exon selection via binding to CU-rich sequence<sup>15,16,35</sup>. Of note, the most 5' end of *Hsf1* exon 7 is CU-rich. To determine whether this sequence is responsive to RBM4-mediated regulation, we generated a mutant (Fig. 7D, diagram). Neither RBM4 overexpression nor NMDA treatment affected the splicing of this mutant (Fig. 7D). Therefore, RBM4 may regulate intron 6 excision via its downstream exonic CU-rich motif. Moreover, this element was sufficient for NMDA-mediated splicing regulation.

Since polypyrimidine tract-binding proteins (PTBP1 and PTBP2) also prefer CU-rich sequences and may antagonize the function of RBM4<sup>35</sup>, we tested whether these two PTB proteins regulate *Hsf1* splicing. Using the *Hsf1* minigene, we observed that overexpression of PTBP1/2 promoted intron 6 retention, in contrast to that observed with RBM4 (Fig. 7E). Therefore, PTBP1/2 may act as a negative regulator for *Hsf1* splicing. We tested whether RBM4 can compete with PTBP1/2 for splicing intron 6. Figure 7F shows that PTBP1/2 increased IR as in Fig. 7E and their effect was reversed by RBM4 in a concentration-dependent manner. Therefore, under developmental cues or neuronal stimulation, the relative concentrations of RBM4 and PTBP1/2 may determine the intron excision of *Hsf1* and subsequent BDNF expression (Fig. 7F, schematic).

## Discussion

Our study of *Rbm4* knockout revealed a pathway and regulatory mechanism for BDNF induction during brain development. As BDNF is key to cerebellar foliation, reactivating the RBM4-regulated pathway could restore icf formation and motor learning in *Rbm4*-deficient cerebella (Fig. 7G).

This study uncovered a critical role of the RBM4–HSF1–BDNF regulatory axis in cerebellar foliation. BDNF deficiency impairs cerebellar foliation<sup>3,19</sup>. The HSF family members play a role in embryonic development and stress response during neurodegenerative pathogenesis<sup>36</sup>. A recent report shows that glutamate receptor signaling activates HSF1 to induce *Bdnf* gene expression<sup>27</sup>. In this study, we demonstrated that RBM4 increased the expression of HSF1 via splicing control, which subsequently transactivated *Bdnf*, indicating a regulatory cascade for BDNF expression (Fig. 3). Moreover, we found that activation of NMDAR provoked the RBM4–HSF1–BDNF pathway by increasing the nuclear abundance of RBM4 (Figs. 5 and 6). This finding revealed that neuronal stimuli modulate alternative splicing via regulating the abundance and subcellular localization of RBM4 (also see below). More importantly, our study demonstrated the function of HSF1 in cerebellar development. HSF1 was downregulated in the *Rbm4* knockout brain. Overexpression of HSF1 almost completely restored BDNF expression, cerebellar foliation, and eventually icf formation (Fig. 4). Notably, either TrkB agonist or HSF1 overexpression can rescue foliation defects and motor learning of *Rbm4*ΔKO cerebellum (Tsai et al.<sup>18</sup>, and this study), indicating that deficiency of BDNF is the primary cause of icf malformation. Although cerebellar morphology was apparently recovered by HSF1, further research is needed to determine whether and how additional RBM4 targets affect neuronal activity, especially those with complete exon inclusion/skipping (Fig. 2B, ΔPSI value of 1.0 or –1.0) or intron retention (Fig. 2D, ΔPIR value of 1.0). For example, *PLPPR4* and *HIVEP2* aberrations have been implicated in neurodevelopmental disorders<sup>37,38</sup>, whether their expression or function is regulated by RBM4 remains to be investigated.

*Hsf1* knockout reduces locomotor activity partly through calbindin reduction<sup>39</sup>, but whether it impairs cerebellar foliation—particularly icf formation—is yet unclear. HSF1 has been implicated in preventing neurodevelopmental disorders and neurodegenerative diseases. It plays a neuroprotective role in developing brains against environmental stressors, as well as in adult brains suffering from polyglutamine-induced neurodegeneration<sup>40–42</sup>. Given that *Rbm4* knockout mice exhibited anxiety<sup>18</sup>, it remains an interesting question as to whether RBM4 aberrations are associated with neuropsychiatric disorders.

In the developing brain, *Rbm4* knockout caused IR in a significant portion of transcripts (Figs. 1 and 2), suggesting that RBM4 regulates gene expression via excision of retained introns. IR has been recognized as an important mechanism for post-transcriptional regulation during cell differentiation or development<sup>43,44</sup>. IR can be determined by epigenetics, transcription rate, and splicing regulator activity<sup>45</sup>. IR may cause degradation of the transcripts in the nucleus or prevent their export to the cytoplasm, leading to downregulation of nonphysiological relevant transcripts<sup>46</sup>. For example, IR is enriched in the transcripts involved in the cell cycle and NF-κB signaling in naive B cells and then downregulated when B cells undergo affinity maturation<sup>26</sup>. In undifferentiated neuroblastoma, PTBP1–

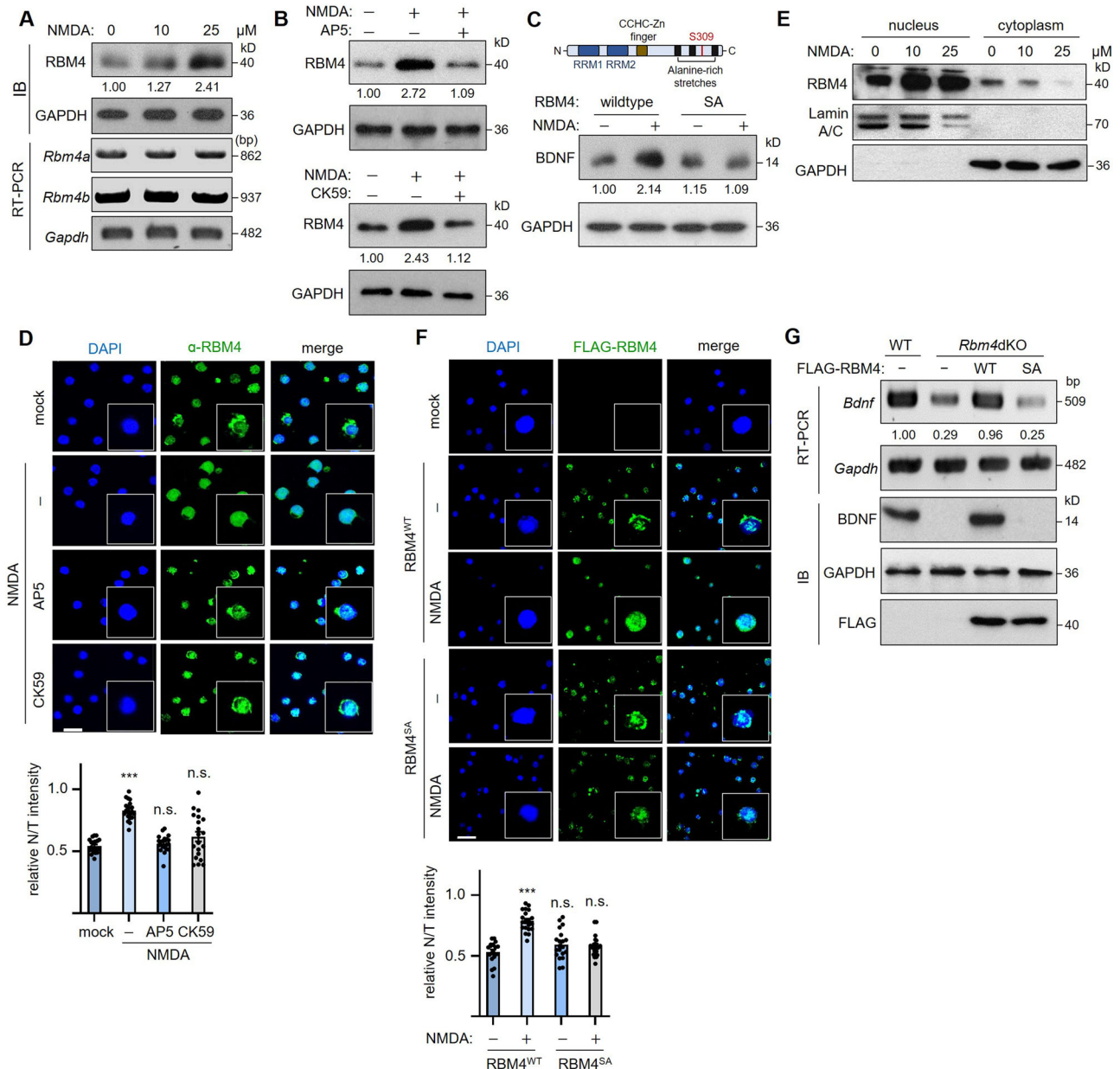


**Fig. 6 | NMDAR signaling stabilizes RBM4 and promotes its nuclear translocation.** **A** GCs were treated with different concentrations of NMDA as in Fig. 5A. Immunoblotting of RBM4 protein and RT-PCR of *Rbm4a/b* mRNA were performed. Folds of RBM4 induction (normalized to GAPDH) were indicated below the blot ( $n = 3$ ). **B** GCs were sequentially treated with AP5 or CK59 and NMDA as in Fig. 5C. E. Immunoblotting of RBM4 and GAPDH was performed. Induction folds were indicated as in (A). **C** Schematic diagram shows the S309A mutant of RBM4. GCs were transiently transfected with the vector expressing FLAG-RBM4 (wild-type or SA) followed by mock or NMDA treatment. Immunoblotting and fold changes were as in (A). **D** GCs were mock or NMDA treated alone or sequentially treated with AP5 or CK59 and NMDA. Immunofluorescence was performed using anti-RBM4. Cells were counterstained with DAPI. The scale bar represents 25 μm. Insets show enlarged images of a representative cell. Bar graph shows the relative ratio of

RBM4 in the nucleus (N) vs. the whole cell (T) (average ± SEM, \*\*\* $P < 0.001$ ). For each group, ~60 cells were measured. Mock was set to 1. **E** Subcellular fractionation was performed in mock or NMDA-treated GCs. Immunoblotting was performed using antibodies against RBM4, Lamin A/C, and GAPDH. **F** GCs were transfected with the vector of FLAG-RBM4 (WT or SA) followed by mock or NMDA treatment. Immunofluorescence was performed using anti-FLAG. No signal was detected in untransfected cells (top panels), indicating the specificity of anti-FLAG. Scale bar, inset, and bar graph were as in (D). For the bar graph, mock-treated RBM4-transfection was set to 1. **G** *Rbm4dKO* GCs were mock-transfected or transfected with the FLAG-RBM4 (WT or SA) vector. RT-PCR and immunoblotting of indicated RNA/protein were performed. Relative *Bdnf* expression levels were indicated ( $n = 3$ ); WT was set to 1.

mediated IR suppresses the expression of synaptic proteins involved in vesicle transport and neurotransmitter release<sup>46</sup>. Downregulation of PTBP1 during neuronal differentiation triggers intron excision and mRNA export to the cytoplasm<sup>46</sup>. Similarly, PTBP1 sequesters the intron-containing transcript of the neuronal gamma-aminobutyric acid (GABA) B receptor (*Gabbr1*) on chromatin and thereby prevents its expression in embryonic stem cells<sup>47</sup>. RBM4 and PTBP1/2 had opposite effects on *Hsf1* intron

excision. RBM4 was able to antagonize the suppressive effect of PTBP1/2 on *Hsf1* intron excision and hence induced BDNF expression (Fig. 7). Moreover, we observed that *Rbm4* knockout increased PTBP1/2 expression (Supplementary Fig. 6). Therefore, it is possible that RBM4 deficiency coupled with PTBP1/2 upregulation results in additive suppression of HSF1 expression. It has been noted that IR is enriched in the transcripts encoding splicing factors and gross changes in splicing factors may further impact



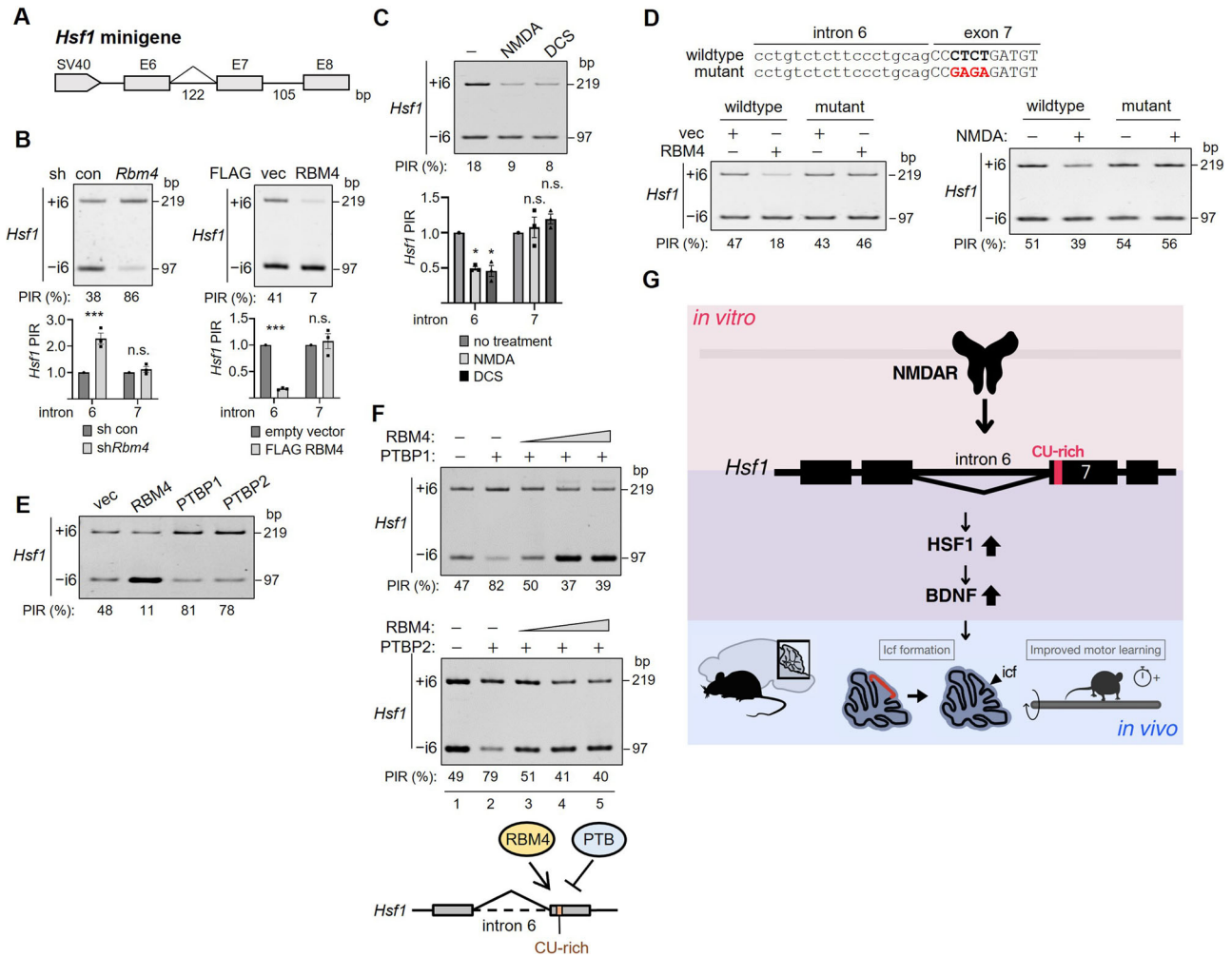


**Fig. 7 | RBM4 regulates *Hsf1* intron excision via a CU-rich motif and antagonizes the negative effect of PTBP1/2.** A Schematic of the *Hsf1* minigene spanning exon 6 to exon 8 of mouse *Hsf1*. SV40 denotes the promoter. B The *Hsf1* minigene and the *Rbm4* shRNA (left panel) or FLAG-RBM4 (right panel) vectors were co-transfected into GCs. RT-PCR was performed to detect intron 6 retention/excision. PIR (%) was indicated below the gels ( $n = 3$ ); PIR measurement was the same in the following panels. Bar graphs show relative PIR of introns 6/7; con shRNA or empty vector was set to 1. C The *Hsf1* minigene was transfected into GCs followed by NMDA or DCS treatment. Bar graph for relative PIR is shown as in (B). D Diagram shows the mutant *Hsf1*, of which nucleotides 3–6 of exon 7 were mutated. GCs were transfected with the wild-type or mutant minigene together with the empty or FLAG-RBM4 vector (left panel) or followed by NMDA

treatment (right panel). E The *Hsf1* minigene was co-transfected with the empty vector (vec) or vector expressing RBM4, PTBP1, or PTBP2. F The *Hsf1* minigene was transfected with the vector of PTBP1 or PTBP2 alone (lane 2) or together with increasing amounts of the RBM4 vector (lanes 3–5). Lane 1 contained the *Hsf1* minigene only. Model shows that RBM4 and PTB proteins may competitively regulate *Hsf1* intron 6 splicing via a CU-rich motif. G Conclusion model: *Rbm4* knockout caused IR of *Hsf1* and hence reduced HSF1 protein level. In vitro results demonstrated that RBM4 promotes intron excision of *Hsf1* via a CU-rich element and hence increased HSF1 and subsequent BDNF expression, and that NMDAR signaling potentiates RBM4 in splicing regulation. In vivo, evidence revealed that HSF1 rescues the foliation defects and motor learning ability of the *Rbm4*KO cerebellum.

IR<sup>25,26</sup>. *Rbm4* knockout also induced IR of many splicing regulators, implicating a pivotal role for RBM4 in splicing regulatory networks. Dynamic IR program is important for erythropoiesis and B cell differentiation<sup>25,26</sup>. Thus, it remains interesting to explore how the dynamics of RBM4-mediated splicing regulation is controlled during brain development.

This study revealed that neuronal activity regulates gene expression via RBM4-mediated intron excision. Signaling-regulated excision of retained introns has been observed in various tissues including erythrocytes, lymphocytes, muscle satellite cells, and neuron<sup>25,26,33,46–51</sup>. For example, upon activation of quiescent satellite cells, the retained intron is removed from the transcripts of the key transcription factors *MyoD* and *Myf5* to initiate muscle differentiation<sup>51</sup>. Phosphorylated oncogenic protein Dek promotes intron excision, but how cellular signaling modulates its activity is still unclear. It has been known for a decade that NMDAR-calmodulin-dependent kinase pathways promote intron excision and nuclear export of the transcripts in the murine-developing brain<sup>50</sup>, indicating IR regulation as one of the critical

mechanisms for development. A more recent report reveals that different forms of neuronal activity differentially regulate intron retention/excision<sup>33</sup>. For example, IR of the *Srsf2* transcript was enhanced by BDNF, but suppressed by GABAergic inhibition<sup>33</sup>. Therefore, neuronal activity can regulate the transcriptome via intron retention/excision. In this study, we demonstrated that stimulation of NMDAR followed by calcium influx and activation of downstream kinases CaMKII and SRPK1 led to stabilization and nuclear accumulation of RBM4 and that RBM4 promoted intron excision likely in a phosphorylation-dependent manner (Fig. 6). Collectively, our results revealed a neuronal stimulation regulated axis in modulating IR.

In conclusion, RBM4 represents a signaling-regulated splicing regulator and promotes intron excision of *Hsf1*, leading to an increase in HSF1 protein levels. HSF1 is critical for BDNF expression and cerebellar foliation. Since dysregulation of BDNF expression is also associated with several neurodevelopmental diseases<sup>52</sup>, activating splicing may offer a potential therapeutic strategy.

## Methods

### **Rbm4 knockout mice**

*Rbm4*dKO mice were previously generated<sup>18</sup>. For experimental use, *Rbm4*dKO mice were obtained by intercrossing between *Rbm4*dKO parents. The parents were obtained from intercross between *Rbm4* double heterozygous (*Rbm4a*<sup>+/-</sup>; *Rbm4b*<sup>+/-</sup>) mice. Genotypes were confirmed by PCR<sup>18</sup>. The mouse experiments (protocol ID: 13-04-547 and 19-12-1370) were approved by the Institutional Animal Care and Use Committee (IACUC) of Academia Sinica and compliant with the Ministry of Science and Technology, Taiwan. The mice were kept in the specific pathogen-free Experimental Animal Facilities, Academia Sinica, and under a 12-h dark/light cycle. Standard chow diet and water were provided *ad libitum*. We have complied with all relevant ethical regulations for animal use.

### **Bioinformatics analysis**

RNA-seq data of E13.5 *Rbm4*dKO embryonic brain were reported<sup>18</sup> (NCBI SRA database with the BioProject accession ID PRJNA980846) and analyzed by using rMATS (<https://rmatseq-mats.sourceforge.io>; version 4.1.2)<sup>53</sup>. Functional annotation of target genes was determined by DAVID<sup>54,55</sup>. For transcriptomic analysis, read counts were normalized using Transcripts Per Million (TPM). Genes with a TPM value of 0 in either wild-type or *Rbm4*dKO groups were excluded. A total of 14,666 genes were analyzed based on the above criteria. Genes with a false discovery rate (FDR) < 0.15 were considered as differentially expressed.

### **Plasmids**

The pDNA3.1-based vectors for expression of FLAG-tagged RBM4 (human RBM4A gene), RBM4-SA mutant, PTBP1, and PTBP2 have been previously described<sup>14,15,34,35</sup>. The HSF1 expression plasmid was purchased from Origene (MR208087). The pLKO.1-shLuc-puro-based *Rbm4* or *Hsf1* shRNA expression vectors were obtained from the National RNAi core facility in Academia Sinica. To generate the *Hsf1* minigene, a genomic DNA fragment encompassing exon 6 to exon 8 of mouse *Hsf1* was obtained by PCR and inserted into the pCH110 vector (Addgene). The CTCT to AGAG mutation was generated by PCR-based mutagenesis. The *Hsf1* coding region was inserted in the frame into the pCAG-DsRed vector (Addgene, #11151) to generate the HSF1-DsRed fusion.

### **Immunoblotting**

Protein extraction was previously described<sup>18</sup>. In brief, homogenized brain/cerebellum tissues were lysed in the radioimmunoprecipitation assay (RIPA) lysis buffer containing 50 mM Tris-HCl, pH 7.3, 150 mM NaCl, 1% nonidet-P40, 0.1% SDS, 0.5% sodium deoxycholate, and protease inhibitors; 1 ml of buffer was used for 20-mg tissues. The supernatant was collected after removing cell debris by centrifugation. For immunoblotting, samples were fractionated on 10% SDS-PAGE and then transferred onto a nitrocellulose membrane (Hybond® ECL™, GERPN303D) and probed with specific primary antibodies, followed by the corresponding horseradish peroxidase-conjugated secondary antibodies (Amersham, NA931; NA934). Signals were detected using Immobilon ECL Substrate (Millipore, WBKLS0500) and X-ray film imaging (FUJIFILM, Super RX-N) and quantified using ImageJ (NIH, version 1.52a).

### **Antibodies**

Antibodies against the following proteins were used: RBM4 (1:1500; ProteinTech, 11614-1-AP), HSF1 (1:1500; Proteintech, 51034-1-AP), hnRNPH1 (1:500; Elabscience, E-AB-65522), hnRNP L (1:500; Elabscience, E-AB-16484), BDNF (1:1000; Abcam, ab108319), FLAG (1:2500; Sigma-Aldrich, F1804), GAPDH (1:3000; ProteinTech, 60004-1-Ig), PTBP1 (1:1000; Abcam, ab133734), PTBP2 (1:1000; Abcam, ab228930), Lamin A/C (1:3000; Sigma-Aldrich, SAB4200236), Calbindin (1:200; Proteintech, 14479-1-AP), Pax6 (1:150; Millipore, AB2237), Akt (1:2000; Cell Signaling Technology, 9272), pAkt (1:1000; Cell Signaling Technology, 9271), ERK1/2 (1:2000; Cell Signaling Technology, 9102), pERK1/2 (1:1000;

Cell Signaling Technology, 9101), CC3 (1:1000; Cell Signaling Technology, 9664), pCREB (1:1000; Proteintech, 28792-1-AP).

### **Hematoxylin-eosin staining**

Paraffin-embedded sections of isolated mouse brain were fixed with 4% paraformaldehyde in phosphate buffer saline (PBS) at pH 7.4 for 24 h, followed by cryoprotection using increasing concentrations of sucrose (ranging from 10% to 30%) in PBS. Brain sections were generated using a Leica CM3050S cryostat and stored at -20 °C. Deparaffinization and rehydration of tissue sections were sequentially performed in the following solutions: xylene and decreasing concentrations (from 100% to 70%) of alcohol, and finally PBS; each step was 5 min. The sections were then stained with Mayer's Hematoxylin for 5 min. The samples were immersed in Stott's tap water for 5 min, followed by 0.5% Eosin Y in 70% alcohol with the addition of 0.2% ice-cold acetic acid for 30 s. Finally, the sections were dehydrated with 95% alcohol, rinsed with xylene, and then applied onto the coverslips.

### **In utero electroporation**

For *in utero* electroporation (IUE), we slightly modified the protocol as described<sup>56</sup>. The pCAG-HSF1-DsRed plasmid (2–3 µl at 5 µg/µl) was injected into the lateral ventricle of the E15.5 mouse brain. The hindbrain region was turned downward for 15 min to allow the solution to diffuse into the fourth ventricle, and then the electrodes were placed close to the bottom for electroporation. Injection of the plasmids (1–2 µl at 5 µg/µl) was also directly performed in the fourth ventricle (Supplementary Fig. 3B). Samples were collected at P0 and P30. Fast Green solution (finally 0.05%) was co-injected for monitoring. The embryo within the uterus was positioned between tweezers-type electrodes with disc electrodes 5 mm in diameter at the tip. Following injection, electronic pulses of 30 V were delivered five times at 950-ms intervals. The uterine horns were then repositioned into the abdominal cavity to allow normal development of the embryos. Throughout the experiments, mice were anesthetized with isoflurane.

### **Culture and transfection of cerebellar granule cells**

The procedure of P7 cerebellar GC isolation was previously described<sup>18</sup>. In brief, the Papain Dissociation System Kit (Worthington, LK003150) was used to isolate GCs. Isolated cerebella were immersed in Calcium/Magnesium-free-PBS-EDTA buffer. Subsequently, the tissues were lysed in papain solution and incubated at 37 °C for 30 min with gentle agitation. The tissues were then mechanically dissociated. GCs were first resuspended in Earle's balanced salt solution containing albumin-ovomuroid inhibitor and DNase (Worthington, LK003150) and then transferred to a fresh tube. After centrifugation, the cell pellet was resuspended in 10% fetal bovine serum-containing medium, filtered through a 70-µm nylon mesh, and seeded in 24-well plates pre-coated with 25 µg/ml of poly-D-lysine. GCs were cultured in serum-free Gibco™ Neurobasal A medium (Thermo Fisher Scientific, 10888022) supplemented with 2% Gibco™ B27 (Thermo Fisher Scientific, 17504044), 2 mM L-glutamine, 1% penicillin/streptomycin (Gibco™, Thermo Fisher Scientific, 10378016), and 150 nM Smoothed agonist (SAG; Sigma-Aldrich, 566661). GCs were maintained in a regular 5% CO<sub>2</sub>-supplemented incubator at 37 °C for further experiments. For splicing assays, about one 1 × 10<sup>6</sup> GCs were transfected with 2 µg of the *Hsf1* minigene and 4 µg of splicing regulator expression vector(s).

Pharmaceutical activation or inhibition of the NMDAR pathways was performed as follows: NMDA (25 µM for 1 h; Sigma-Aldrich, M3262) or DCS (50 µM for 1 h; Sigma-Aldrich, C6880), AP5 (25 µM for 30 min; Sigma-Aldrich, A8054), EGTA (2 mM for 30 min; Sigma-Aldrich, E3889), CK59 (500 nM for 30 min; Millipore, 208922-M), or SRPIN340 (30 µM for 15 min; MedChemExpress, HY-13949). Inhibitors were treated prior to the addition of NMDA.

### **RNA extraction and RT-PCR**

RNA was extracted from the mouse brain using TRIzol reagent (Thermo Fisher Scientific, 15596018) according to the manufacturer's instructions.

Addition of 1/5 volume of chloroform (Merck Millipore, 67-66-3) followed by centrifugation caused phase separation. RNA was precipitated with isopropanol and ethanol. For reverse transcription (RT), 1 µg of RNA was hybridized with 0.3 µg oligo(dT) and converted to cDNA by using the SuperScript™ III First-strand Synthesis System (Thermo Fisher Scientific, 18080-044). PCR was performed using specific primers (Supplementary Table 1) using Taq polymerase. Real-time quantitative PCR (qPCR) was performed in triplicate using PerfeCTa qPCR SuperMix (Quantabio, 95050-500) on the LightCycler® 480 Instrument II (Roche Applied Science). Data was normalized against *GAPDH*.

### Rotarod test

Rotarod test was performed using the Rota-Rod apparatus (47600 Rota-Rod, Ugo Basile, Italy) according to the procedure described previously<sup>18</sup>. For each group, ten 6-week-old mice were tested. Four trials of pretraining (4 rpm for 60 s) were performed with a 10-min inter-trial interval. For the testing, mice were forced to run on a rod accelerating from 4 to 40 rpm in 300 s with an interval of 15 min.

### Statistics and reproducibility

Sample sizes were not predetermined using statistical methods. Statistical analyses were conducted using the Student's *t*-test or one-way analysis of variance (ANOVA) with at least three independent experimental groups to evaluate the significance between treatments. Standard deviation (SD) and standard error of the mean (SEM) were computed using Microsoft Excel, and data visualization was performed using GraphPad Prism 9.5.1 and Integrative Genomics Viewer (IGV). Statistical significance was defined as \**P* < 0.05, \*\**P* < 0.01, and \*\*\**P* < 0.001. Unless otherwise specified, error bars represent SEM. Details of sample sizes are provided in the figure legends or corresponding figure panels. The gel images without statistical analysis below were all reproduced at least three times.

### Reporting summary

Further information on research design is available in the Nature Portfolio Reporting Summary linked to this article.

### Data availability

The alternative splicing events identified by rMATS are provided in Supplementary Data 1. Numerical data points underlying all graphs are available in the Supplementary Data 2. Uncropped images of gels and blots for this study are presented in Supplementary Fig. 7. The RNA sequencing result is deposited and available at the NCBI SRA database (BioProject accession ID: PRJNA980846). All other supporting data of this study are available from the corresponding author upon reasonable request.

Received: 6 February 2024; Accepted: 27 November 2024;

Published online: 30 December 2024

### References

- Baralle, F. E. & Giudice, J. Alternative splicing as a regulator of development and tissue identity. *Nat. Rev. Mol. Cell Biol.* **18**, 437–451 (2017).
- Montes, M., Sanford, B. L., Comiskey, D. F. & Chandler, D. S. RNA splicing and disease: animal models to therapies. *Trends Genet.* **35**, 68–87 (2019).
- Schwartz, P. M., Borghesani, P. R., Levy, R. L., Pomeroy, S. L. & Segal, R. A. Abnormal cerebellar development and foliation in *BDNF*<sup>-/-</sup> mice reveals a role for neurotrophins in CNS patterning. *Neuron* **19**, 269–281 (1997).
- Licatalosi, D. D. et al. *Ptbp2* represses adult-specific splicing to regulate the generation of neuronal precursors in the embryonic brain. *Genes Dev.* **26**, 1626–1642 (2012).
- Raj, B. & Blencowe, B. J. Alternative splicing in the mammalian nervous system: recent insights into mechanisms and functional roles. *Neuron* **87**, 14–27 (2015).
- Vuong, C. K., Black, D. L. & Zheng, S. The neurogenetics of alternative splicing. *Nat. Rev. Neurosci.* **17**, 265–281 (2016).
- Calarco, J. A. et al. Regulation of vertebrate nervous system alternative splicing and development by an SR-related protein. *Cell* **138**, 898–910 (2009).
- Quesnel-Vallières, M. et al. Misregulation of an activity-dependent splicing network as a common mechanism underlying autism spectrum disorders. *Mol. Cell.* **64**, 1023–1034 (2016).
- Quesnel-Vallières, M., Irimia, M., Cordes, S. P. & Blencowe, B. J. Essential roles for the splicing regulator nSR100/SRRM4 during nervous system development. *Genes Dev.* **29**, 746–759 (2015).
- Zheng, S. et al. PSD-95 is post-transcriptionally repressed during early neural development by PTBP1 and PTBP2. *Nat. Neurosci.* **15**, 381–388 (2012).
- Vuong, J. K. et al. PTBP1 and PTBP2 serve both specific and redundant functions in neuronal pre-mRNA splicing. *Cell Rep.* **17**, 2766–2775 (2016).
- Feng, H. et al. Complexity and graded regulation of neuronal cell-type-specific alternative splicing revealed by single-cell RNA sequencing. *Proc. Natl Acad. Sci. USA* **118**, e2013056118 (2021).
- Arora, R. et al. Spatial transcriptomics reveals distinct and conserved tumor core and edge architectures that predict survival and targeted therapy response. *Nat. Commun.* **14**, 5029 (2023).
- Tarn, W. Y. et al. RBM4 promotes neuronal differentiation and neurite outgrowth by modulating Numb isoform expression. *Mol. Biol. Cell.* **27**, 1676–1683 (2016).
- Su, C. H., Hung, K. Y., Hung, S. C. & Tarn, W. Y. RBM4 regulates neuronal differentiation of mesenchymal stem cells by modulating alternative splicing of pyruvate kinase M. *Mol. Cell Biol.* **37**, e00466–16 (2017).
- D, D., Hung, K. Y. & Tarn, W. Y. RBM4 modulates radial migration via alternative splicing of *Dab1* during cortex development. *Mol. Cell Biol.* **38**, e00007–e00018 (2018).
- Su, C. H., D, D. & Tarn, W. Y. Alternative splicing in neurogenesis and brain development. *Front. Mol. Biosci.* **5**, 12 (2018).
- Tsai, Y. Y., Shen, C. L., D, D., Tsai, C. Y. & Tarn, W. Y. Activation of TrkB signaling mitigates cerebellar anomalies caused by *Rbm4*-*Bdnf* deficiency. *Commun. Biol.* **6**, 910 (2023).
- Courchesne, E., Yeung-Courchesne, R., Press, G. A., Hesselink, J. R. & Jernigan, T. L. Hypoplasia of cerebellar vermal lobules VI and VII in autism. *N. Engl. J. Med.* **318**, 1349–1354 (1988).
- Brini, M., Cali, T., Ottolini, D. & Carafoli, E. Neuronal calcium signaling: function and dysfunction. *Cell Mol. Life Sci.* **71**, 2787–2814 (2014).
- Braunschweig, U. et al. Widespread intron retention in mammals functionally tunes transcriptomes. *Genome Res.* **24**, 1774–1786 (2014).
- Lipscombe, D. & Lopez Soto, E. J. Alternative splicing of neuronal genes: new mechanisms and new therapies. *Curr. Opin. Neurobiol.* **57**, 26–31 (2019).
- Iijima, T. et al. *SAM68* regulates neuronal activity-dependent alternative splicing of neurexin-1. *Cell* **147**, 1601–1614 (2011).
- Saltzman, A. L. et al. Regulation of multiple core spliceosomal proteins by alternative splicing-coupled nonsense-mediated mRNA decay. *Mol. Cell Biol.* **28**, 4320–4330 (2008).
- Pimentel, H. et al. A dynamic intron retention program enriched in RNA processing genes regulates gene expression during terminal erythropoiesis. *Nucleic Acid Res.* **44**, 838–851 (2016).
- Ullrich, S. & Guigó, R. Dynamic changes in intron retention are tightly associated with regulation of splicing factors and proliferative activity during B-cell development. *Nucleic Acids Res.* **48**, 1327–1340 (2020).
- Franks, H. et al. Heat shock factor HSF1 regulates BDNF gene promoters upon acute stress in the hippocampus, together with pCREB. *J. Neurochem.* **165**, 131–148 (2023).
- Ni, J. Z. et al. Ultraconserved elements are associated with homeostatic control of splicing regulators by alternative splicing and nonsense-mediated decay. *Genes Dev.* **21**, 708–718 (2007).

29. Ge, Y. & Porse, B. T. The functional consequences of intron retention: alternative splicing coupled to NMD as a regulator of gene expression. *Bioessays* **36**, 236–243 (2014).
30. Farrant, M., Feldmeyer, D., Takahashi, T. & Cull-Candy, S. G. NMDA-receptor channel diversity in the developing cerebellum. *Nature* **368**, 335–339 (1994).
31. Mony, L. & Paoletti, P. Mechanisms of NMDA receptor regulation. *Curr. Opin. Neurobiol.* **83**, 102815 (2023).
32. Favaron, M. et al. NMDA-stimulated expression of BDNF mRNA in cultured cerebellar granule neurones. *Neuroreport* **4**, 1171–1174 (1993).
33. Mazille, M., Buczak, K., Scheiffele, P. & Mauger, O. Stimulus-specific remodeling of the neuronal transcriptome through nuclear intron-retaining transcripts. *EMBO J.* **41**, e110192 (2022).
34. Lin, J. C., Hsu, M. & Tarn, W. Y. Cell stress modulates the function of splicing regulatory protein RBM4 in translation control. *Proc. Natl Acad. Sci. USA* **104**, 2235–2240 (2007).
35. Lin, J. C. & Tarn, W. Y. RBM4 down-regulates PTB and antagonizes its activity in muscle cell-specific alternative splicing. *J. Cell Biol.* **193**, 509–520 (2011).
36. Kim, H. & Gomez-Pastor, R. HSF1 and its role in Huntington's disease pathology. *Adv. Exp. Med. Biol.* **1410**, 35–95 (2023).
37. Srivastava, S. et al. Loss-of-function variants in HIVEP2 are a cause of intellectual disability. *Eur. J. Hum. Genet.* **24**, 556–561 (2016).
38. Li, H. et al. PLPPR4 haploinsufficiency causes neurodevelopmental disorders by disrupting synaptic plasticity via mTOR signalling. *J. Cell Mol. Med.* **27**, 3286–3295 (2023).
39. Ingenwerth, M., Estrada, V., Stahr, A., Müller, H. W. & von Gall, C. HSF1-deficiency affects gait coordination and cerebellar calbindin levels. *Behav. Brain Res.* **310**, 103–108 (2016).
40. Uchida, S. et al. Impaired hippocampal spinogenesis and neurogenesis and altered affective behavior in mice lacking heat shock factor 1. *Proc. Natl Acad. Sci. USA* **108**, 1681–1686 (2011).
41. Kondo, N. et al. Heat shock factor-1 influences pathological lesion distribution of polyglutamine-induced neurodegeneration. *Nat. Commun.* **4**, 1405 (2013).
42. Hashimoto-Torii, K. et al. Roles of heat shock factor 1 in neuronal response to fetal environmental risks and its relevance to brain disorders. *Neuron* **82**, 560–572 (2014).
43. Grabski, D. F. et al. Intron retention and its impact on gene expression and protein diversity: a review and a practical guide. *Wiley Interdiscip. Rev. RNA* **12**, e1631 (2021).
44. Joglekar, A. et al. A spatially resolved brain region- and cell type-specific isoform atlas of the postnatal mouse brain. *Nat. Commun.* **12**, 463 (2021).
45. Monteuis, G., Wong, J. J. L., Bailey, C. G., Schmitz, U. & Rasko, J. E. J. The changing paradigm of intron retention: regulation, ramifications and recipes. *Nucleic Acids Res.* **47**, 11497–11513 (2019).
46. Yap, K., Lim, Z. Q., Khandelia, P., Friedman, B. & Makeyev, E. V. Coordinated regulation of neuronal mRNA steady-state levels through developmentally controlled intron retention. *Genes Dev.* **26**, 1209–1223 (2012).
47. Iannone, C. et al. PTBP1-activated co-transcriptional splicing controls epigenetic status of pluripotent stem cells. *Mol. Cell.* **83**, 203–218.e209 (2023).
48. Yue, L., Wan, R., Luan, S., Zeng, W. & Cheung, T. H. Dek modulates global intron retention during muscle stem cells quiescence exit. *Dev. Cell.* **53**, 661–676.e666 (2020).
49. Bell, T. J. et al. Intron retention facilitates splice variant diversity in calcium-activated big potassium channel populations. *Proc. Natl Acad. Sci. USA* **107**, 21152–21157 (2010).
50. Mauger, O., Lemoine, F. & Scheiffele, P. Targeted intron retention and excision for rapid gene regulation in response to neuronal activity. *Neuron* **92**, 1266–1278 (2016).
51. Yeom, K. H. et al. Tracking pre-mRNA maturation across subcellular compartments identifies developmental gene regulation through intron retention and nuclear anchoring. *Genome Res.* **31**, 1106–1119 (2021).
52. Camuso, S., La Rosa, P., Fiorenza, M. T. & Canterini, S. Pleiotropic effects of BDNF on the cerebellum and hippocampus: implications for neurodevelopmental disorders. *Neurobiol. Dis.* **163**, 105606 (2022).
53. Shen, S. et al. rMATS: robust and flexible detection of differential alternative splicing from replicate RNA-Seq data. *Proc. Natl Acad. Sci. USA* **111**, E5593–E5601 (2014).
54. Huang da, W., Sherman, B. T. & Lempicki, R. A. Systematic and integrative analysis of large gene lists using DAVID bioinformatics resources. *Nat. Protoc.* **4**, 44–57 (2009).
55. Sherman, B. T. et al. DAVID: a web server for functional enrichment analysis and functional annotation of gene lists. *Nucleic Acids Res.* **50**, W216–w221 (2022).
56. Saito, T. & Nakatsuji, N. Efficient gene transfer into the embryonic mouse brain using in vivo electroporation. *Dev. Biol.* **240**, 237–246 (2001).

## Acknowledgements

We appreciate Guey-Shin Wang and Yi-Shuian Huang (Academia Sinica, Taipei, Taiwan) for the materials and discussion. We also thank Experimental Animal Facilities, Pathology Core, and Common Equipment Core Facility of the Institute of Biomedical Sciences for their technical assistance. This study was supported by Grant 112WIA011015 from the National Science and Technology Council of Taiwan to W.-Y.T.

## Author contributions

C.-L.S. designed and performed all experiments, interpreted the data, and contributed to manuscript preparation. Y.-Y.T. initiated this study, generated the plasmid for *in utero* electroporation, and participated in the discussion. S.-J.C. guided *in utero* electroporation. Y.-M.C. performed RNA-seq data analysis. W.-Y.T. conceived the study, supervised the experiments, and wrote the manuscript.

## Competing interests

The authors declare no competing interests.

## Additional information

**Supplementary information** The online version contains supplementary material available at <https://doi.org/10.1038/s42003-024-07328-6>.

**Correspondence** and requests for materials should be addressed to Woan-Yuh Tarn.

**Peer review information** *Communications Biology* thanks Tomoko Yamada and the other, anonymous, reviewers for their contribution to the peer review of this work. Primary Handling Editors: Alex Nord and Christina Karlsson Rosenthal. A peer review file is available.

**Reprints and permissions information** is available at <http://www.nature.com/reprints>

**Publisher's note** Springer Nature remains neutral with regard to jurisdictional claims in published maps and institutional affiliations.

**Open Access** This article is licensed under a Creative Commons Attribution-NonCommercial-NoDerivatives 4.0 International License, which permits any non-commercial use, sharing, distribution and reproduction in any medium or format, as long as you give appropriate credit to the original author(s) and the source, provide a link to the Creative Commons licence, and indicate if you modified the licensed material. You do not have permission under this licence to share adapted material derived from this article or parts of it. The images or other third party material in this article are included in the article's Creative Commons licence, unless indicated otherwise in a credit line to the material. If material is not included in the article's Creative Commons licence and your intended use is not permitted by statutory regulation or exceeds the permitted use, you will need to obtain permission directly from the copyright holder. To view a copy of this licence, visit <http://creativecommons.org/licenses/by-nc-nd/4.0/>.

© The Author(s) 2024